Journal of Computational Physics 228 (2009) 2552–2565

Contents lists available at ScienceDirect

Journal of Computational Physics

journal homepage: www.elsevier.com/locate/jcp

Simulation of solid–fluid mixture flow using moving particle methods

Shuai Zhang *, Shigeyuki Kuwabara, Takahito Suzuki, Yoshio Kawano, Koji Morita, Kenji Fukuda

Department of Applied Quantum Physics and Nuclear Engineering, Kyushu University, 744 Moto-oka, Nishi-ku, Fukuoka 819-0395, Japan

ARTICLE INFO

Article history:
Received 23 June 2008
Received in revised form 11 November 2008
Accepted 9 December 2008
Available online 24 December 2008

Keywords:
Moving particle methods
Finite volume particle (FVP) method
Distinct element method (DEM)
Fluid–solid mixture flows

ABSTRACT

A new basic framework for solid–fluid mixture flow simulation was developed using moving particle methods. The interactions between solid and fluid were modeled by the finite volume particle (FVP) method. The distinct element method (DEM) together with a multi-time-step algorithm was introduced into the FVP method to calculate the effects of contact between solid bodies and between solid bodies and walls. The introduced DEM model was verified by experimental analyses for the collapse of multiple solid cylinder layers. The proposed algorithm using the optimized DEM model was then applied to a water dam breaking, involving multiple solid cylinder layers. A comparison between experiments and simulations demonstrated the DEM model introduced into the FVP method is effective in representing solid–fluid mixture flows reasonably well.

1. Introduction

Numerical studies on fluid–solid mixture flows are needed for understanding many phenomena in engineering fields. It would be difficult for conventional Eulerian mesh methods to directly simulate such complicated flows since it is necessary to capture or track fluid–solid interphase. Recently, several particle methods have been developed for numerical simulations. Among them, moving particle methods, based on the fully Lagrangian framework, are more appropriate for fluid–solid interphase simulations because the interphase is always clearly represented in calculations.

There are several kinds of moving particle methods for describing fluid dynamics, such as smoothed particle hydrodynamics (SPH) [1], the moving particle semi-implicit (MPS) method [2] and the finite volume particle (FVP) method [3], which was introduced in detail in our paper [4]. It is worth to note that there is a moving particle method with a similar name as FVP method, referred to the finite-volume particle method (FVPM), which was developed on the basis of numerical flux functions for compressible flows [5]. In these methods, the calculation region is occupied by discrete moving particles and thus a mesh grid is unnecessary. It has been verified that they are able to simulate continuous fluids with satisfactory results; e.g., the methods have been applied to shock tubes [6], water dam breakage [7] and impact of a liquid droplet falling into a liquid pool [4]. Unlike mesh methods, there is no need for interphase construction in the moving particle methods, because each phase can be represented by moving particles with specific physical properties. Therefore, the application of moving particle methods to solid–fluid mixture flows is straightforward.

There has been successful numerical modeling of the interactions of a single solid body with fluid using moving particle methods. For example, the MPS method together with the passively moving solid (PMS) model has been used to simulate a solid float in breaking waves [2] and a ship profile being hit by a wave has been simulated using the particle finite element method [8]. These studies show that moving particle methods might be powerful tools in the direct simulation of fluid–solid mixture flows without interface tracking between phases.

* Corresponding author. Tel./fax: +81 92 802 3499.
E-mail addresses: zhang@nucl.kyushu-u.ac.jp, shuai.zhang@gmail.com (S. Zhang).

0021-9991/$ - see front matter © 2008 Elsevier Inc. All rights reserved.
doi:10.1016/j.jcp.2008.12.005

As far as we know, there is limited, if any, published work on more complicated numerical simulations of fluid flow with multiple solid bodies using moving particle methods. The present study aims to build a basic framework for such numerical simulations and validate the framework with experiments. First, the algorithm for simulating interactions between fluid and one solid body, mentioned above [2], is realized using the FVP method. We then investigate how to include the collision forces between solid bodies and between a solid body and a wall in the developed computer code using the FVP method. As a well-known fully Lagrangian numerical method for granular flow simulations, the distinct element method (DEM) [9] is an appropriate choice to calculate the forces in the FVP framework.

However, a typical DEM calculation requires a much smaller time step compared with the FVP method. To cope with this problem, a multiple time-step scheme is developed for the FVP and DEM coupling calculations, with each method using a different time-step size. In addition, the size of a solid body would be much larger than that of a typical moving fluid particle in some engineering applications. The present study undertakes a basic investigation by making two-dimensional simulations of solid bodies with uniform shape. Multiple moving particles are used to represent a solid body in the simulations. The DEM calculation is implemented for each solid body, while the FVP calculation is carried out for all moving particles.

Finally, code verifications are carried out using two series of experiments. First, the introduced DEM model is validated for the collapse of multiple solid cylinder layers. Water dam breakage with multiple solid cylinder layers is then investigated to verify the proposed framework for solid–fluid mixture flow simulations.

2. Numerical methods

2.1. Governing equations for fluid–solid mixture flows

The governing equations for incompressible fluid are

$$\begin{cases} \nabla \cdot \vec{u} = 0 \\ \frac{D\vec{u}}{Dt} = -\frac{(\nabla p)_{ll}}{\rho_l} + \frac{\nabla(\mu \cdot \nabla \vec{u})_{ll}}{\rho_l} + \frac{\vec{f}_{sl}}{\rho_l} + \frac{\vec{f}_{others}}{\rho_l} \end{cases} \tag{1}$$

where $\vec{u}$, p and ρ_l are the velocity, pressure and density of a fluid particle, respectively, μ is the dynamic viscosity, $(\nabla p)_{ll}$ and $\nabla(\mu \cdot \nabla \vec{u})_{ll}$ are the pressure and viscosity forces within the fluid phase, respectively, $\vec{f}_{sl}$ is the interaction force between fluid and solid phases, and $\vec{f}_{others}$ are other volume forces, such as gravity.

The governing equations for solid bodies are

$$\begin{cases} m\frac{D\vec{u}}{Dt} = \vec{F}_{col} + \vec{f}_{ls}V + \vec{F}_{others} \\ I\frac{D\vec{\omega}}{Dt} = T_{col} + T_{ls} + T_{others} \end{cases} \tag{2}$$

where $\vec{u}, \vec{\omega}, m, V$ and I are the translation velocity, rotation velocity, mass, volume and inertia of a solid body, respectively. $\vec{F}_{col}$ and T_{col} are the force and torque, respectively, caused by collisions between solid bodies and collisions of solid bodies with solid walls, $\vec{f}_{ls}$ and T_{ls} are the volume force and torque, respectively, caused by interactions between fluid and solid phases, and $\vec{F}_{others}$ and T_{others} are other forces and torques, respectively, for example those due to gravity.

2.2. Overview of the FVP method

In the present study, we choose the FVP method because it has been verified as being very stable numerically, especially for free surface flow simulations [10]. In the FVP method, the control volume of one moving particle is assumed as a circle in two-dimensional simulations [4]:

$$V = \pi R^2 = (\Delta l)^2 \tag{3}$$

where V, R and Δl are the particle control volume, radius of the particle control volume and initial particle distance, respectively. According to Gauss's law, the gradient and Laplacian operators are expressed by

$$\nabla\phi = \lim_{R\to 0}\frac{1}{V}\oint_V \nabla\phi dV = \lim_{R\to 0}\frac{1}{V}\oint_S \phi\vec{n}dS \tag{4}$$

$$\nabla^2\phi = \lim_{R\to 0}\frac{1}{V}\oint_V \nabla^2\phi dV = \lim_{R\to 0}\frac{1}{V}\oint_S \nabla\phi\cdot\vec{n}dS \tag{5}$$

where ϕ is an arbitrary scalar function, and S and V are the particle surface area and volume, respectively. S and V are equivalent to $2\pi R$ and πR^2 in a two-dimensional system, respectively.

As a result, in the FVP method the gradient and Laplacian terms can be approximated as [4]

$$\langle\nabla\phi\rangle_i = \left\langle\frac{1}{V}\oint_S \phi\vec{n}dS\right\rangle_i = \frac{1}{V}\sum_{j\neq i}\left(\phi_i + \frac{\phi_j - \phi_i}{|\vec{r}_{ij}|}R\right)\vec{n}_{ij}\Delta S_{ij} \tag{6}$$

$$\langle \nabla^2 \phi \rangle_i = \left\langle \frac{1}{V} \oint_S \nabla \phi \cdot \vec{n} dS \right\rangle_i = \frac{1}{V} \sum_{j \neq i} \left(\frac{\phi_j - \phi_i}{|\vec{r}_{ij}|} \frac{\vec{r}_{ij}}{|\vec{r}_{ij}|} \right) \cdot \vec{n}_{ij} \Delta S_{ij} \tag{7}$$

where the interaction surface of particle j with particle i, ΔS_{ij}, can be calculated by

$$\Delta S_{ij} = \frac{w_{ij}}{n^0} S \tag{8}$$

with the initial number density of the particles, n^0. The number density of particle i can be calculated as

$$n_i = \sum_{j \neq i} w_{ij} \tag{9}$$

The value of n^0 is set to the number density of a particle which is not near or on boundaries. The unit vector of the distance between two particles, $\vec{n}_{ij}$, is expressed by

$$\vec{n}_{ij} = \vec{r}_{ij} / |\vec{r}_{ij}| = (\vec{r}_j - \vec{r}_i) / |\vec{r}_{ij}| \tag{10}$$

where $\vec{r}_i$ and $\vec{r}_j$ are the positions of particles i and j, respectively.

The kernel function w_{ij} is defined as [4]

$$w_{ij} = \sin^{-1}(R/|\vec{r}_{ij}|) - \sin^{-1}(R/r_e) \tag{11}$$

where r_e is the cut-off radius and is usually chosen as $3.1\Delta l$. Fig. 1 is a schematic diagram of neighboring particles around particle i within the cut-off radius. If the distance between two particles is larger than the cut-off radius, the kernel function is set as zero.

Using Eqs. (8)–(10), Eqs. (6) and (7) can be rearranged as

$$\langle \nabla \phi \rangle_i = \frac{S}{V n^0} \sum_{j \neq i} \left(\phi_i + \frac{\phi_j - \phi_i}{|\vec{r}_{ij}|} R \right) w_{ij} \frac{\vec{r}_{ij}}{|\vec{r}_{ij}|} \tag{12}$$

$$\langle \nabla^2 \phi \rangle_i = \frac{S}{V n^0} \sum_{j \neq i} \frac{\phi_j - \phi_i}{|\vec{r}_{ij}|} w_{ij} \tag{13}$$

Using the gradient and Laplacian models, the governing equations for fluids can be easily discretized. Fig. 2 is a flowchart of the FVP calculation. The pressure implicit with splitting of operators (PISO) algorithm [11] is applied to the FVP method. Calculations are separated into prediction and correction stages [4]. In the prediction stage, particles move with guessed velocities to temporal positions

$$\vec{r}^* = \vec{r}^n + \Delta t_{FVP} \cdot \vec{u}^* \tag{14}$$

where $\vec{u}^*$ is the guessed velocity and its value is initially set to $\vec{u}^n$, $\vec{r}^*$ and $\vec{r}^n$ are temporal and previous positions, respectively, and Δt_{FVP} is the time step size in the FVP calculation.

On the temporal positions, the governing equations for incompressible fluids can be approximated as

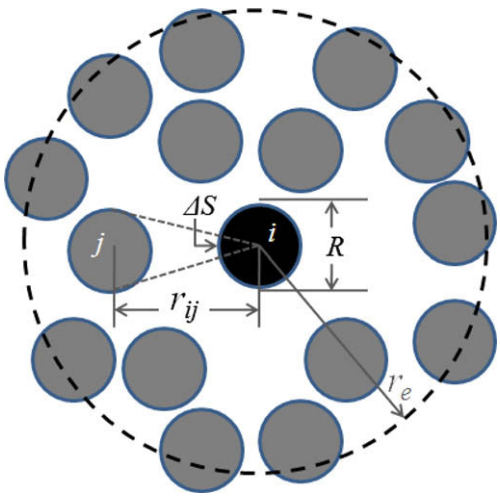

Fig. 1. Neighboring particles around particle i within the cut-off radius.

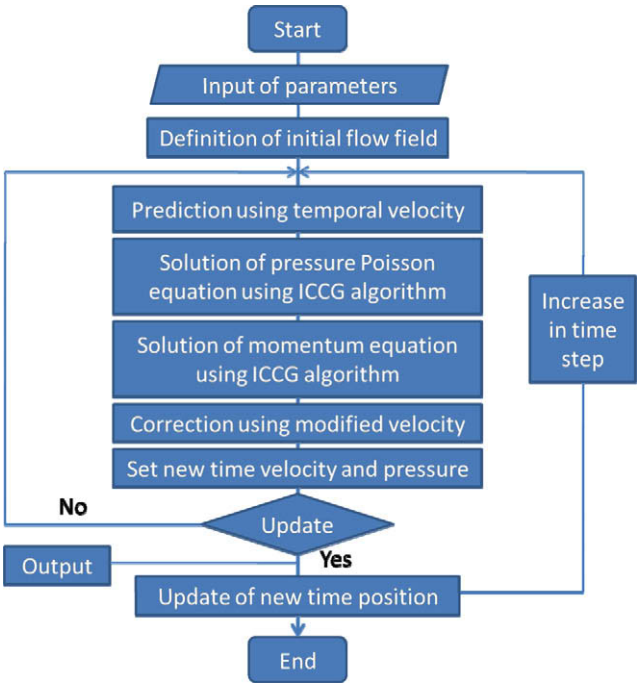

Fig. 2. Flowchart of the FVP calculation.

$$\frac{\vec{u}^{**}-\vec{u}^{n}}{\Delta t_{FVP}} = -\frac{1}{\rho}\nabla p^{**} + \frac{1}{\rho}\nabla\cdot\mu\nabla\vec{u}^{**} + \frac{\vec{f}^{**}_{others}}{\rho} \tag{15}$$

$$\nabla\cdot\vec{u}^{**} = 0 \tag{16}$$

where superscript $**$ means new time step values. Combing Eqs. (15) and (16), a pressure Poisson equation can be obtained as

$$\nabla\cdot\left(\frac{1}{\rho}\nabla p^{**}\right) = \frac{\nabla\cdot\vec{u}^{n}}{\Delta t_{FVP}} \tag{17}$$

The above equation should be rearranged into an appropriate form for multi-phase flow simulations. Since the pressure forces between two interacting particles are equal to each other, the following approximation can be obtained:

$$\frac{\nabla p^{**}_{ij}}{\rho_i} = \frac{\nabla p^{**}_{ji}}{\rho_j} = \frac{p^{**}_S - p^{**}_i}{\rho_i|\vec{r}_{ij}|/2} = \frac{p^{**}_j - p^{**}_S}{\rho_j|\vec{r}_{ij}|/2} \tag{18}$$

where p^{**}_i and p^{**}_j are the pressures of particles i and j, respectively, p^{**}_S is the pressure on the surface between two particles, and ∇p^{**}_{ij} is the pressure forces acting on particle i and given by particle j. After arrangement, Eq. (18) can be changed into

$$\frac{\nabla p^{**}_{ij}}{\rho_i} = \frac{2}{\rho_i+\rho_j}\frac{p^{**}_j - p^{**}_i}{|\vec{r}_{ij}|} \tag{19}$$

The resultant form of the left-hand side of the Poisson equation is expressed by

$$\left\langle\nabla\cdot\left(\frac{1}{\rho}\nabla p^{**}\right)\right\rangle_i = \frac{S}{Vn^0}\sum_{j\neq i}\frac{2}{\rho_i+\rho_j}\frac{p^{**}_j - p^{**}_i}{|\vec{r}_{ij}|}w_{ij} \tag{20}$$

In the correction stage, Eq. (17) is solved via the incomplete Cholesky conjugate gradient (ICCG) method. The obtained pressure p^{**} is used to solve the momentum equation implicitly. The resultant velocity $\vec{u}^{**}$ is used again as the guessed velocities $\vec{u}^{*}$ in the prediction stage. This iterative procedure usually needs only three iterations for one time step to obtain results with satisfactory accuracy [4].

In the FVP calculation, the time-step size Δt_{FVP} is taken according to the Courant–Friedrichs–Lewy condition:

$$\max\left\{\frac{abs[(\vec{u}_j-\vec{u}_i)\cdot\vec{n}]\Delta t_{FVP}}{|\vec{r}_{ij}|}\right\} < \varepsilon \tag{21}$$

where *abs*[·] means absolute value, and ε is usually chosen as 0.2. If the above condition is not satisfied, the half value of the previous time-step size is used [4].

2.3. Overview of the DEM model

In the present study, we formulate the DEM calculation for solid bodies of the same diameter in two-dimensional systems. Therefore, they are modeled as cylinders with a unit length. If the distance between the mass centers of two solid bodies is less than their diameters, they are defined as being in contact. Otherwise, the collision force between two bodies is assumed to be zero.

The DEM model is described schematically in Fig. 3. The collision effects between two solids are modeled by a spring and dashpot, which represent elastic and damping forces, respectively. The slide represents a switch for the maximum static friction force. In addition to the global coordinate (x,y), a local coordinate (ξ,η) is constructed for solid *ii* for convenience of calculation. The two-dimensional collision force of solid body *ii* received from solid body *jj*, $\vec{F}_{jj\to ii} = (F_{\xi,jj\to ii}, F_{\eta,jj\to ii})$, is calculated in DEM as [12]

$$\begin{cases} F_{\xi,jj\to ii}(t) = e_n(t) + d_n(t) \\ e_n(t) = e_n(t-\Delta t_{DEM}) + k_n \Delta\xi_{ii,jj} \\ d_n(t) = c_n \frac{\Delta\xi_{ii,jj}}{\Delta t_{DEM}} \end{cases} \tag{22}$$

$$\begin{cases} F_{\eta,jj\to ii}(t) = e_s(t) + d_s(t) \\ e_s(t) = e_s(t-\Delta t_{DEM}) + k_s \Delta\eta_{ii,jj} \\ d_s(t) = c_s \frac{\Delta\eta_{ii,jj}}{\Delta t_{DEM}} \end{cases} \tag{23}$$

where Δt_{DEM} is the time-step size of the DEM calculation. The following conditions apply to the collision force

$$F_{\xi,jj\to ii}(t) = F_{\eta,jj\to ii}(t) = 0 \quad \text{for } e_n(t) \leqslant 0 \tag{24}$$

$$|F_{\eta,jj\to ii}(t)| = \mu \cdot |e_n(t)| \quad \text{for } |e_s(t)| > \mu e_n(t) \tag{25}$$

where $F_{\eta,jj\to ii}(t)$ has the same sign as $e_s(t)$. Eq. (24) states there is no contact effect with negative elastic force, which means that two solids detach from each other. Eq. (25) is a switch between static and dynamic friction forces.

In Eqs. (22) and (23), e_n and e_s are the elastic forces in normal and tangent directions, respectively, d_n and d_s are the damping forces in normal and tangent directions, respectively, k_n and k_s are the stiffnesses in normal and tangent directions, respectively, and c_n and c_s are the damping coefficients in normal and tangent directions, respectively. The relationships between the DEM parameters [12] are

$$k_s = \frac{k_n}{2(1+\upsilon)} \tag{26}$$

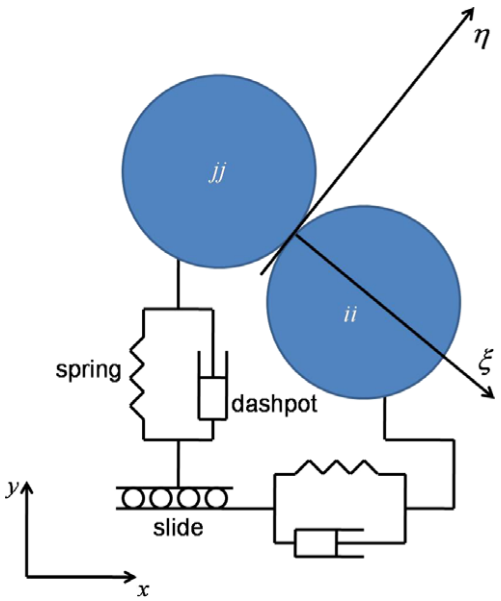

Fig. 3. Schematic description of the DEM model.

$$c_n = \alpha_{cn} \cdot 2\sqrt{mk_n} \tag{27}$$

$$c_s = \frac{c_n}{\sqrt{2(1+\upsilon)}} \tag{28}$$

where m is the mass of a solid body, υ is the Poisson ratio, α_{cn} is the tuning parameter, μ is the maximum static friction coefficient, and ξ and η are the local coordinates in normal and tangent directions, respectively. The relationship between the global and local coordinates is expressed for $\Delta\xi_{ii,jj}$ and $\Delta\eta_{ii,jj}$, which are the increases in distance between two solid centers in the normal and stress directions, respectively [12]:

$$\begin{bmatrix} \Delta\xi_{ii,jj} \\ \Delta\eta_{ii,jj} \end{bmatrix} = M_{ii} \begin{bmatrix} u_{ii} - u_{jj} \\ v_{ii} - v_{jj} \end{bmatrix} \Delta t_{DEM} + \begin{bmatrix} 0 & 0 \\ \omega_{c,ii} & \omega_{c,jj} \end{bmatrix} \begin{bmatrix} R_{ii} \\ R_{jj} \end{bmatrix} \Delta t_{DEM} \tag{29}$$

where $[u,v]$ and ω_c are the solid's translation velocity vector and rotation velocity, respectively, and $\omega_c$is positive in the anticlockwise direction. R_{ii} and R_{jj} are the diameters of solids ii and jj, respectively, and M_{ii} is the translation matrix between global and local coordinates. In two-dimensional systems, $M_{ii}$is calculated as

$$M_{ii} = \begin{bmatrix} \cos(\omega_{c,ii}\Delta t_{DEM}) & -\sin(\omega_{c,ii}\Delta t_{DEM}) \\ \sin(\omega_{c,ii}\Delta t_{DEM}) & \cos(\omega_{c,ii}\Delta t_{DEM}) \end{bmatrix} \tag{30}$$

The collision force acting on solid body ii is calculated as a summation of all forces applied by neighboring solid bodies that are in contact with solid body ii:

$$\vec{F}_{col,ii} = \sum_{jj} \vec{F}_{jj \to ii} \tag{31}$$

In addition, to keep numerical stability in the DEM calculation, it is recommended that [13]

$$\Delta t_{DEM} = \frac{2\pi}{\alpha_{tn}} \sqrt{\frac{m}{k_n}} \tag{32}$$

where α_{tn} is the model parameter, which will be optimized by experimental analyses in the present study. Eq. (32) enables us to choose an appropriate value for the normal stiffness from a given time-step size of the DEM calculation. As a result, a larger time-step size can be applied without losing the characteristic behaviors of solid movements. The flowchart for the DEM calculation is shown in Fig. 4.

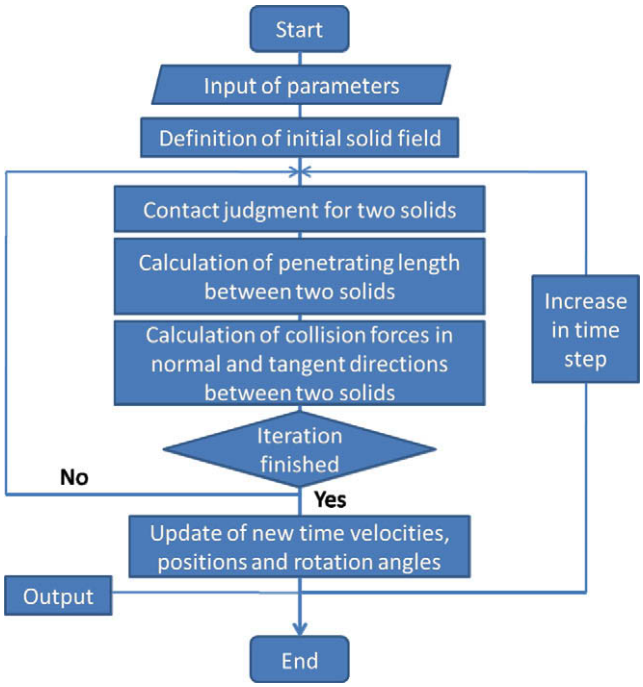

Fig. 4. Flowchart of the DEM calculation.

2.4. Coupling algorithm for solid–fluid mixture flow simulation

The FVP method and DEM model together with the PMS model [2] are coupled to directly simulate the solid–fluid mixture flows. Since the diameters of solid bodies would be larger than those of the moving particles, multiple moving particles are used to represent one solid body. In addition, the FVP method and DEM model applied in the present study use fully explicit and fully implicit algorithms, respectively. As a result, the characteristic time-step size of the DEM calculation should be much smaller than that of the FVP calculation. To cope with this problem, a multiple time-step algorithm is introduced. The procedure for coupling the FVP and DEM calculations is described schematically in Fig. 5.

First, all moving particles are assumed as fluid particles and included in the FVP calculation, which is the same treatment as in the MPS simulation with the PMS model [2]. Thereafter, the velocities and pressures of fluid particles are updated. For the moving particles representing solid bodies, the PMS model [2] is applied to calculate the translation and rotation velocities of each solid body:

$$\vec{u}^{**}_{c,ii} = \frac{1}{N}\sum_{i=1}^{N}\vec{u}^{*}_{i} \tag{33}$$

$$\vec{\omega}^{**}_{c,ii} = \vec{\omega}^{n}_{c,ii} + \frac{1}{I_{ii}}\sum_{i=1}^{N} m_i(\vec{r}^{n}_{i} - \vec{r}^{n}_{c,ii}) \times (\vec{u}^{*}_{i} - \vec{u}^{n}_{i}) \tag{34}$$

where m_i is the mass of solid particle i, $\vec{u}^{*}$ is the velocity of the solid moving particle after the FVP calculation, $\vec{u}^{**}_{c}$ and $\vec{\omega}^{**}_{c}$ are the translation and rotation velocities of solid bodies, respectively, N is the number of the solid particles representing the solid body ii, $\vec{r}^{n}_{i}$ is the position of solid moving particles, which belong to solid body ii in the previous time step, and $\vec{\omega}^{n}_{c}$ is the rotation velocity of solid bodies in the previous time step. The inertia I of the rigid solid body is calculated as

$$I_{ii} = \sum_{i=1}^{N} m_i(\vec{r}^{n}_{i} - \vec{r}^{n}_{c,ii})^2 \tag{35}$$

and the mass center $\vec{r}^{n}_{c}$ of the solid body in the previous time step is calculated as

$$\vec{r}^{n}_{c,ii} = \frac{1}{N}\sum_{i=1}^{N}\vec{r}^{n}_{i} \tag{36}$$

Thereafter, the solid moving particle's position and velocity are modified as

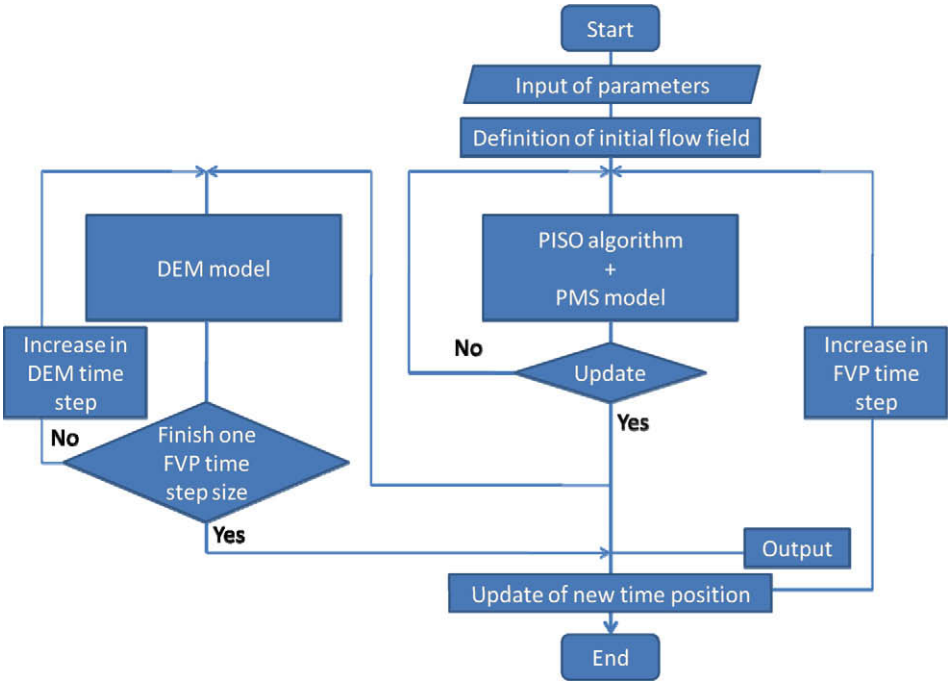

Fig. 5. Schematic description of the coupling algorithm for the FVP and DEM calculations.

$$\vec{r}_i^{**} = \vec{r}_i^n + M_{ii}(\vec{r}_i^n - \vec{r}_{c,ii}^n) \tag{37}$$

$$\vec{u}_i^{**} = \frac{\vec{r}_i^{**} - \vec{r}_i^n}{\Delta t_{FVP}} \tag{38}$$

The interaction force between fluid and solid phases at this time step can be thus represented by the pressure and stress forces between solid and fluid particles using the PMS model:

$$\vec{f}_{sl} = -(\nabla p)_{ls} + \nabla(\mu \cdot \nabla \vec{u})_{ls} \tag{39}$$

If there is only one solid interacting with fluid, the new time-step value for positions and velocities of solid moving particles is then updated using Eqs. (37) and (38). In the present study, the DEM calculation is then performed for each solid body to simulate the collision effects. The increases in distances $\Delta\xi$ and $\Delta\eta$ are calculated from $\vec{u}_c^{**}$ and $\vec{\omega}_c^{**}$ with Eqs. (29), (33) and (34). The collision force between solid bodies is then solved using Eqs. (22), (23) and (31). Correspondingly, the velocities of solid bodies are calculated as

$$\vec{u}_{c,ii}^{n,k+1} = \vec{u}_{c,ii}^{n,k} + \Delta t_{DEM} \frac{\vec{F}_{col,ii}^{n,k}}{m_{ii}} \tag{40}$$

$$\vec{\omega}_{c,ii}^{n,k+1} = \vec{\omega}_{c,ii}^{n,k} + \Delta t_{DEM} \frac{T_{col,ii}^{n,k}}{I_{ii}} \tag{41}$$

where k is the number of time steps in the DEM calculation and n is the time step of the FVP calculation, and m_{ii} is the mass of the solid body. The initial values of $\vec{u}_c^{n,0}$ and $\vec{\omega}_c^{n,0}$ are equal to $\vec{u}_c^{**}$ and $\vec{\omega}_c^{**}$, respectively.

Using translation and rotation velocities, the rotation angle and mass center of the solid body are updated as

$$\vec{r}_{c,ii}^{n,k+1} = \vec{r}_{c,ii}^{n,k} + \Delta t_{DEM} \vec{u}_{c,ii}^{n,k+1} \tag{42}$$

$$\vec{\theta}_{ii}^{n,k+1} = \vec{\theta}_{ii}^{n,k} + \Delta t_{DEM} \vec{\omega}_{c,ii}^{n,k+1} \tag{43}$$

where $\vec{r}_c^{n,0}$ and $\theta^{n,0}$ are equal to $\vec{r}_c^n$ and $\vec{\theta}^n$, respectively. The position and velocity of the solid particle are updated as

$$\vec{r}_i^{n,k+1} = \vec{r}_i^{n,k} + M_{ii}(\vec{r}_i^{n,k} - \vec{r}_{c,ii}^{n,k}) \tag{44}$$

$$\vec{u}_i^{n,k+1} = \frac{\vec{r}_i^{n,k+1} - \vec{r}_i^{n,k}}{\Delta t_{DEM}} \tag{45}$$

where $\vec{r}^{n,0}$ is equal to $\vec{r}^n$.

Finally, after the DEM calculations are performed till $\Delta t_{FVP} = (k+1)\Delta t_{DEM}$ is satisfied, the position and velocity of the solid moving particle are updated as

$$\vec{r}_i^{n+1} = \vec{r}_i^{n,k+1} \tag{46}$$

$$\vec{u}_i^{n+1} = \vec{u}_i^{n,k+1} \tag{47}$$

3. Numerical simulations

3.1. Verification of the DEM model

As mentioned above, all the parameters in the DEM calculation can be determined with the DEM time-step size Δt_{DEM} and adjustable parameters, α_{tn} and α_{cn}, using Eqs. (26)–(28), (32). To verify this approach and determine the appropriate adjustable parameters, experimental analyses were performed for the collapse of multiple solid cylinder layers.

Fig. 6 is a photograph of the experimental setup for the collapse of solid cylinder layers. Solid cylinders were initially piled up as several layers on the observers' left in an acrylic resin tank with a length of 26 cm, a width of 10 cm and a height of 26 cm. The solid cylinders were made of aluminum and had a density of 2.7×10^3 kg/m^3, diameter of 1.0 cm and length of 9.9 cm. The initial stationary state of the cylinder layers was maintained by a plate that could be withdrawn. The number of aluminum cylinder layers was an experimental parameter and 6, 8, 10 and 12 layers were selected. Solid layers with five or six cylinders were alternately piled up between the left wall of the tank and the plate, which was 6 cm from the wall. After the plate was quickly removed vertically upwards, the cylinder layers began collapsing owing to gravity and the cylinders ran toward the right wall of the tank. The transient behavior of the cylinder layers was recorded by a high speed camera shooting at 200 frames per second.

A preliminary numerical study was performed to tune the adjustable parameter α_{tn} using a Poisson ratio of 0.3, maximum static friction coefficients of 0.3 and a time step set as 1.0×10^{-6} s. In this simulation, the penetration length between two solid bodies during collision was investigated. The adjustable parameter α_{tn} was fixed as 300 with a maximum penetration length of less than 1% of the solid body's diameter. To determine an appropriate value for the adjustable parameter α_{cn}, the DEM simulations for the collapse of aluminum cylinder layers were performed in a two-dimensional system by neglecting

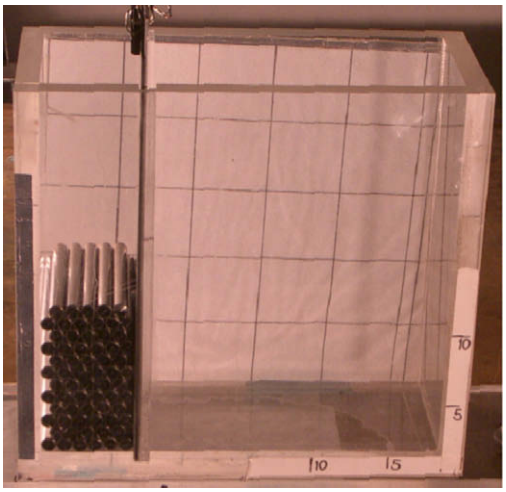

Fig. 6. Experiment setup for the collapse of solid cylinder layers (12 layer case).

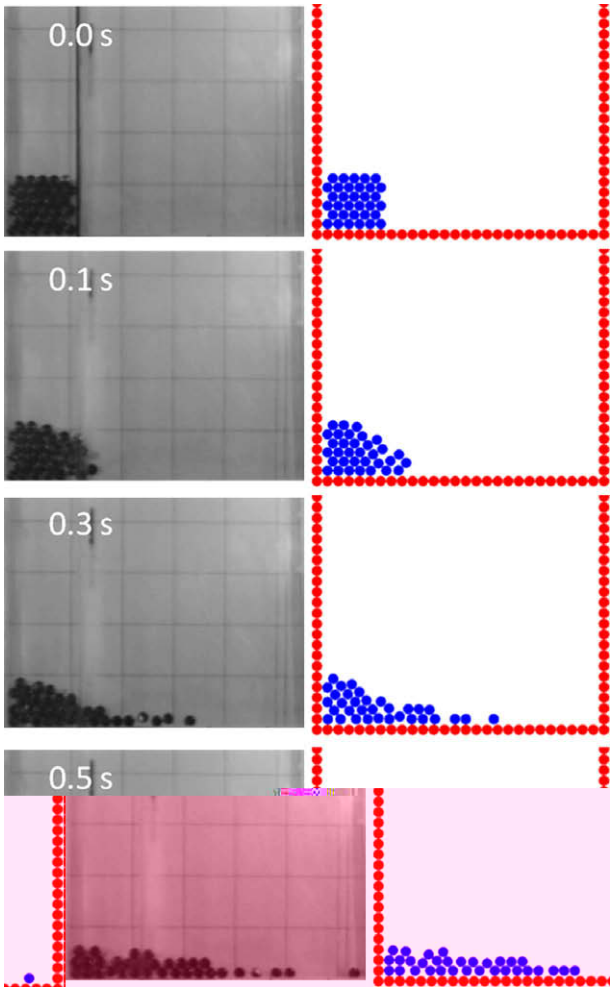

Fig. 7. Transient behavior of a six cylinder layer collapse (left column: experiment; right column: simulation).

the front and back walls of the tank. The stiffness and damping coefficients of the walls were set to those of aluminum. α_{cn} was thus tuned as 0.3.

In the DEM simulations for the collapse of aluminum cylinder layers, the initial collision forces were set as zero for all cylinders. The collapse of the cylinder layers was simulated after settling of the cylinders for 1.0 s. This treatment was necessary since the cylinders were not in contact with each other initially. The contacting length is much longer than the moving particle diameter. As a result, it is difficult to define the contacting length for each solid cylinder initially. In the following discussions, the time zero is defined by the removal of the withdrawal plate.

The transient behavior and average of the mass centers of the cylinders were compared with the experimental results. The mass center average was calculated using

$$\vec{r}_{aver} = \frac{1}{N}\sum_{ii=1}^{N}\vec{r}_{c,ii}, \tag{48}$$

where N is the number of cylinders and $\vec{r}_{c,ii}$ is the mass center of cylinder ii. Figs. 7 and 8 show the simulation results in the case of six layers of cylinders compared with experimental results. The present DEM calculations well represented the experimental results. The simulated transient behavior of the layer collapse agrees well with the experimental results, as can be seen in Fig. 7. Fig. 8 shows good agreement between simulation and experimental mass center averages, the latter obtained by averaging the results for five experiment runs.

From these results, it can be concluded that the present approach enables us to determine the DEM parameters reasonably well. In addition, the DEM time-step size used in the present simulations can be much larger than a typical DEM time step, which would be about approximately 1.0×10^{-8}–1.0×10^{-9} s in the present cases. This is useful in improving the efficiency of DEM calculations.

3.2. Verification of solid–fluid mixture flows

The breaking of a water dam involving multiple solid cylinder layers was used to verify the proposed coupling algorithm for the FVP and DEM calculations. The experimental data for verification were obtained using the same experimental setup as that used for verification of the DEM model, although the cylinder layers were submerged in water. The water dam height was set at 12 cm, and 6, 8, 10 and 12 cylinder layers were used.

For the present solid–fluid mixture flow simulations, two-dimensional calculations were also performed. The density and dynamic viscosity of water were set as 1000 kg/m^3 and 1.0×10^{-3} m^2/s, respectively. The initial distance between moving particles was 1 mm. One cylinder was represented by 69 moving solid particles. The initial moving particle arrangement is shown in Fig. 9 for the case of six cylinder layers. The FVP and DEM time-step sizes were chosen as 1.0×10^{-4} s and 1.0×10^{-6} s, respectively. In the present DEM calculation, the stiffness and damping coefficients were the same as those used in the previous simulation of the collapse of solid cylinder layers. The plate to be withdrawn was represented by moving particles in one layer. The layer was pulled vertically upward at a velocity of 2.0 m/s. After settling of the cylinders in the water dam for 1.0 s, the breaking of the water dam involving solid cylinder layers was simulated. In the following discussions, time zero corresponds to the start of the withdrawal of the plate. Simulations with and without use of the DEM model were carried out and compared with experiments to determine the effect of the collision forces between solid phases.

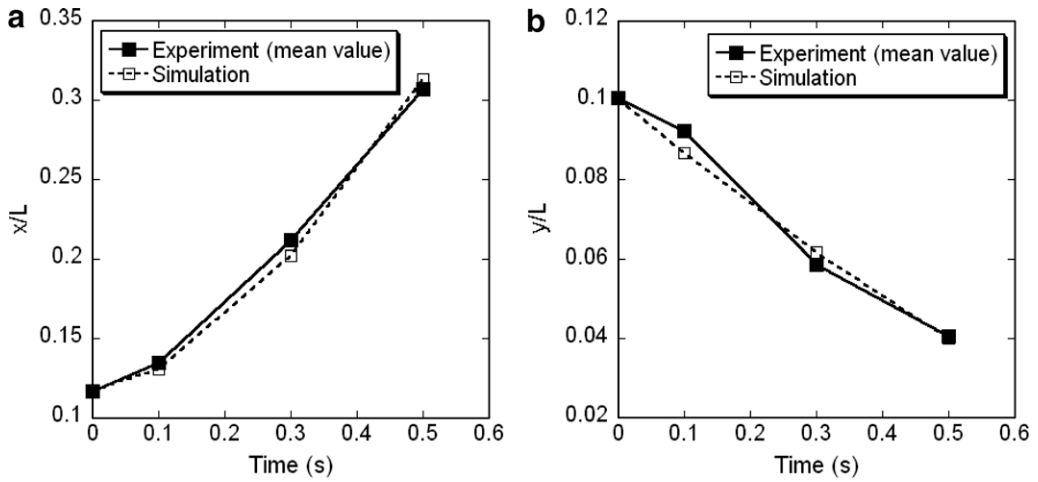

Fig. 8. Transient average of mass centers of cylinders in a six cylinder layer collapse (a) in the horizontal direction and (b) in the vertical direction (x and y are the positions of the mass center in horizontal and vertical directions, respectively; L is the length of the tank).

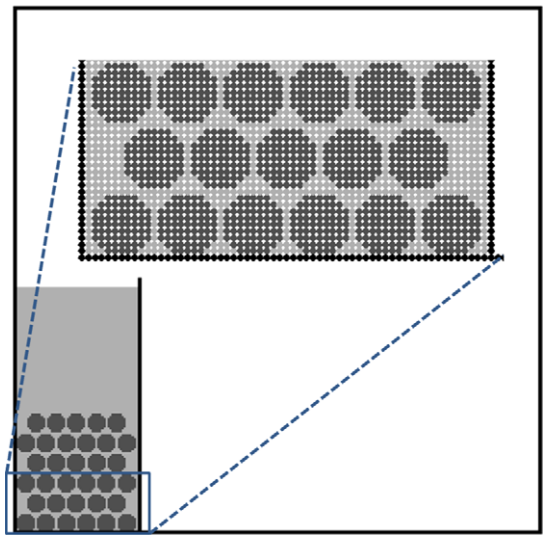

Fig. 9. Initial particle arrangement for simulation of water dam breakage with six solid cylinder layers.

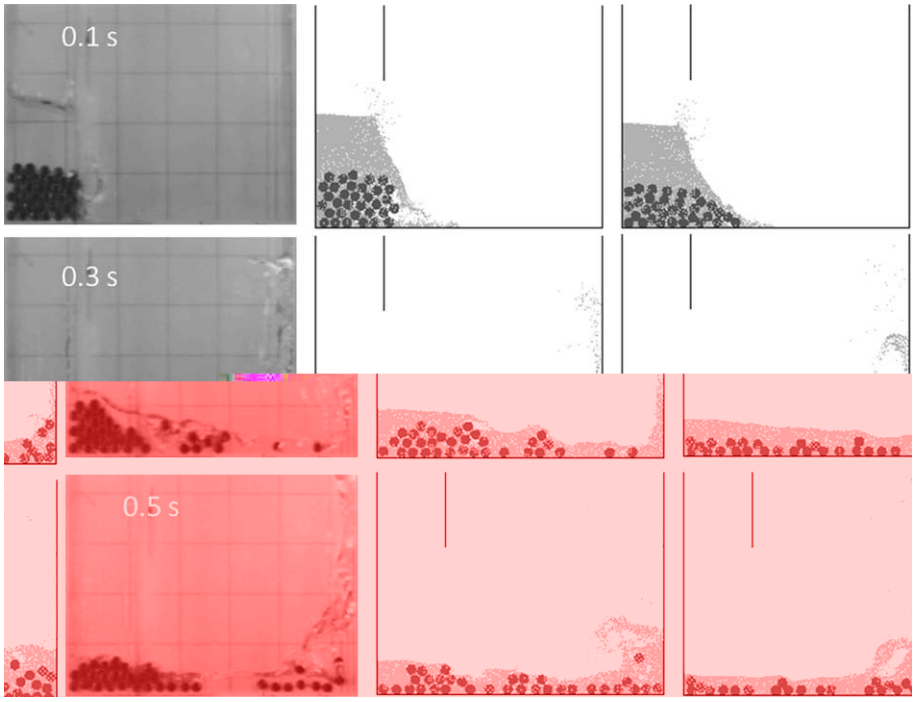

Fig. 10. Transient behavior of water dam breakage with six solid cylinder layers (left column: experiment; center column: FVP simulation using the DEM model; right column: FVP simulation not using the DEM model).

Figs. 10 and 11 show the comparison of transient mixture flow behaviors for the simulation and experiment in the cases of six and twelve cylinder layers, respectively. It can be clearly seen that the simulations with and without use of the DEM model are quite different. This difference seems reasonable. The collision forces simulated by the DEM model between cylinders and walls of the tank retard the movements of the mixture flow. To check this point, as shown in Fig. 12, the arriving time, which corresponds to the first instance of a cylinder coming into contact with the right wall of the tank, was compared for the simulations and experiments. The arriving times obtained by the simulations using the DEM model and the experiments were around 0.35 s, while those obtained by the simulation not using the DEM model was around 0.25 s. Though the

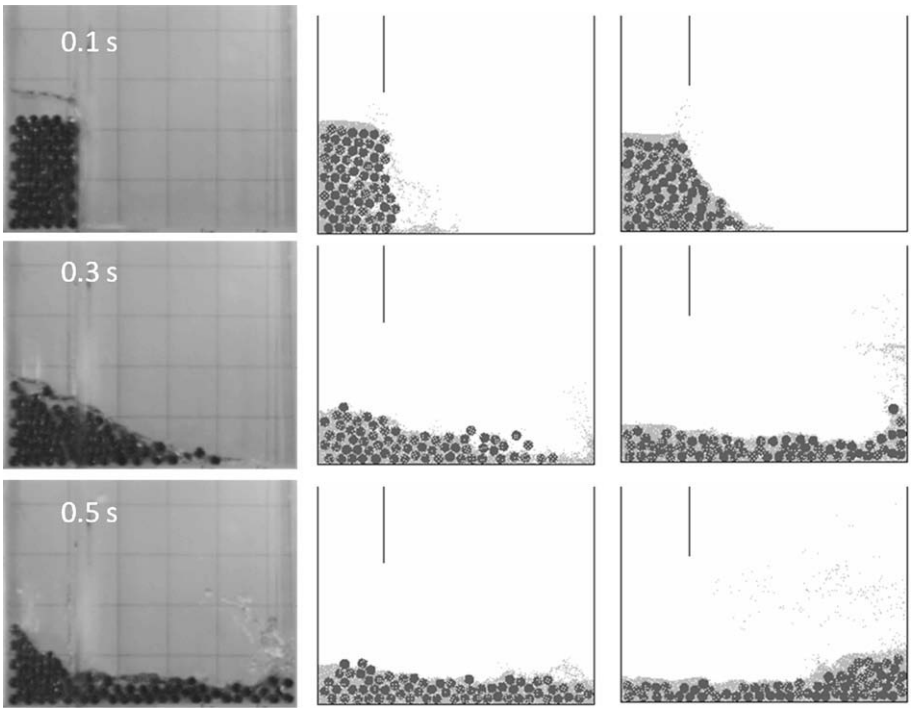

Fig. 11. Transient behavior of water dam breakage with 12 solid cylinder layers (left column: experiment; center column: FVP simulation using the DEM model; right column: FVP simulation not using the DEM model).

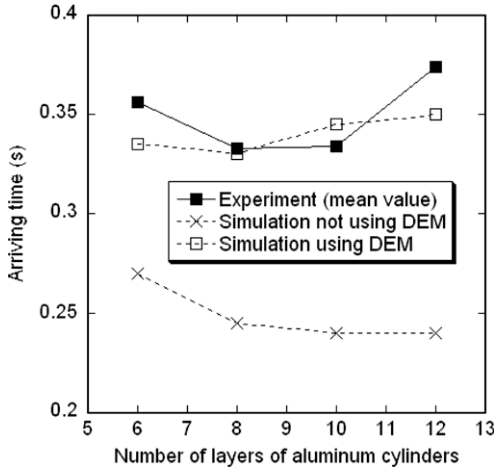

Fig. 12. Comparison of the arriving times between FVP simulations using/not using the DEM model and experimental results.

simulations using the DEM model were not in complete agreement with the experiments regarding the arriving time, it can be said the DEM model improves the results of the FVP simulations.

In addition, the characteristic behaviors of the cylinder movement in the mixture flow were well represented by the simulations using the DEM model. For convenience, in Fig. 13, the initial arrangement of the six layers of cylinders in the water dam is marked schematically by an upper-left oval, an upper-right oval and a central triangle. A comparison of the mixture flows in the tank at 0.35 s for the experiment and simulation using the DEM model is shown in Fig. 14. In both the experiment and simulation, characteristic behaviors are seen in the cylinder movement. The upper-right cylinders detach from the cylinder cluster and then bounce on the bottom wall. The upper-left cylinders drop to the bottom-left corner of the tank and then spread laterally. The central cylinders move together and maintain their triangular formation till they fully spread on the bottom wall. Such phenomena cannot be simulated by the calculations without using the DEM model.

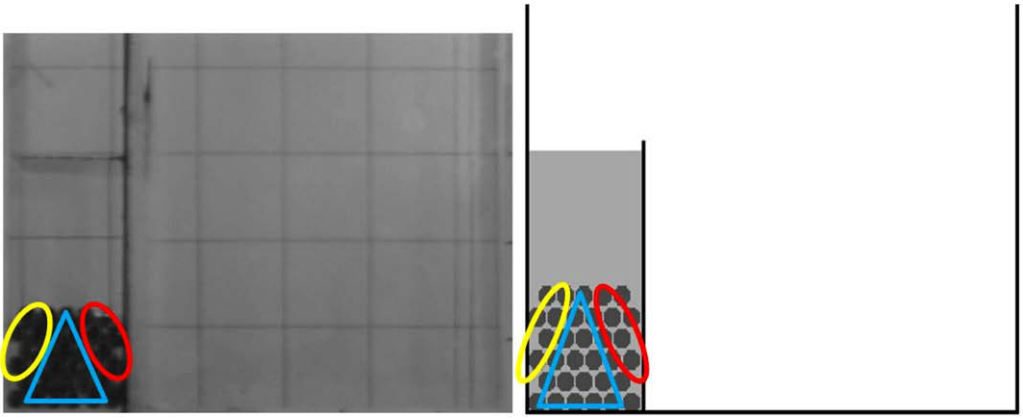

Fig. 13. Initial arrangement of the six-layer cylinders in a water dam (left: experiment; right: simulation).

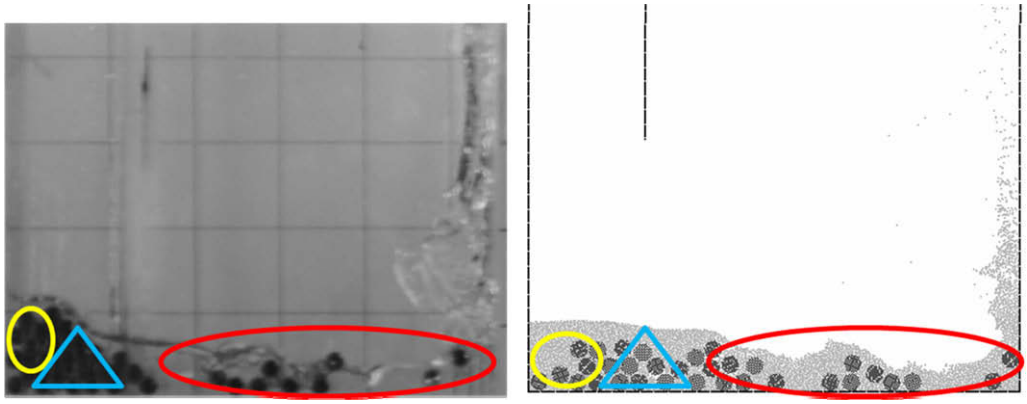

Fig. 14. Mixture flow behaviors after the water dam breakage with six cylinder layers at 0.35 s (left: experiment; right: simulation using DEM model).

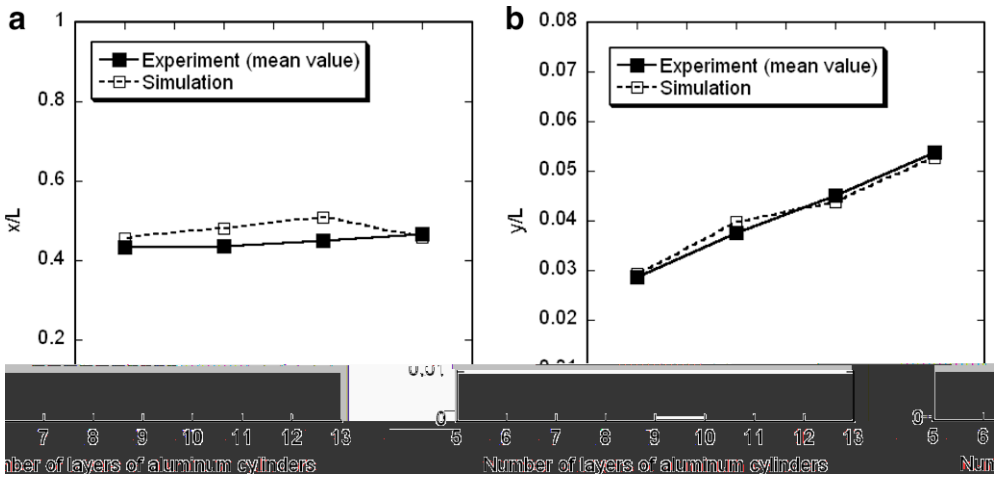

Fig. 15. Static average of mass centers of cylinders after the water dam break (a) in the horizontal position and (b) in the vertical position (x and y are the positions of mass center in horizontal and vertical directions, respectively; L is the length of the tank).

In Fig. 15 the static average centers of mass of the cylinders after the mixture flow settled are compared for the experiments and simulations using the DEM model for the cases with different numbers of cylinder layers. The experimental results were the mean measurement of five runs. It can be said that the present simulation using the DEM model represents the static state of the mixture flow after the water dam breaks reasonably well by comparison with the experimental result.

4. Conclusions

In this study, a coupling algorithm for FVP and DEM calculations was proposed and verified. Numerical simulations of experiments in which multiple solid cylinder layers collapsed were performed to validate the approach for defining appropriate parameters in the DEM calculations. The present DEM simulations reproduced the experimental results well under the present experimental conditions. Thereafter, the proposed algorithm was applied to the simulation of a water dam breaking, involving multiple solid cylinder layers. The FVP simulation using the DEM model reasonably represented the transient behavior of the solid–fluid mixture flow by comparison with the experiments. As a result, it can be concluded that a basic framework for the moving particle method was successfully developed for solid–fluid mixture flow simulations. Although the present numerical method was formulated for solid phase with uniform and two-dimensionally symmetrical shape, its extension to three-dimensional systems might enable us to treat arbitrary solid shapes by introducing the DEM calculation to each moving particle representing the solid phase.

References

[1] J.J. Monaghan, Smoothed particle hydrodynamics, Rep. Progr. Phys. 68 (2005) 1703.
[2] S. Koshizuka, A. Nobe, Y. Oka, Numerical analysis of breaking waves using the moving particle semi-implicit method, Int. J. Numer. Meth. Fluid 26 (1998) 751.
[3] K. Yabushita, S. Hibi, A finite volume particle method for an incompressible fluid flow, Proc. Comput. Eng. Conf. 10 (2005) 419 (in Japanese).
[4] S. Zhang, K. Morita, K. Fukuda, N. Shiarakawa, A new algorithm for surface tension model in moving particle methods, Int. J. Numer. Meth. Fluid 55 (2007) 225.
[5] D. Hietel, K. Steiner, J. Struckmeier, A finite-volume particle method for compressible flows, Math. Models Methods Appl. 10 (2000) 1362.
[6] J.J. Monaghan, R.A. Gingold, Shock simulation by the particle method SPH, J. Comput. Phys. 52 (1983) 374.
[7] S. Koshizuka, Y. Oka, Moving-particle semi-implicit method for fragmentation of incompressible fluid, Nucl. Sci. Eng. 123 (1996) 421.
[8] S.R. Idelsohn, E. Onate, K. Yabushita, F. Del Pin, N. Calvo, Fluid-structure interaction using the particle finite element method, Comput. Meth. Mech. Eng. 195 (2006) 2100.
[9] P.A. Cundall, O.D.L. Strack, A discrete numerical model for granular assemblies, Geotechnique 29 (1979) 47.
[10] S. Zhang, Development of moving particle methods for computational fluid dynamics, Ph.D thesis, University of Kyushu, 2006.
[11] R.I. Issa, Solution of the implicitly discretised fluid flow equations by operator-splitting, J. Comput. Phys. 62 (1985) 40.
[12] H. Gotoh, T. Sakai, Numerical simulation of sheetflow as granular material, J. Wtrwy. Port. Coast. Oc. Eng. 123 (1997) 329.
[13] H. Gotoh, E. Harada, T. Sakai, Optimization of parameters in DEM-based numerical movable bed simulator, J. Jpn. Soc. Civil Eng. 691 (2001) 159 (in Japanese).